This is a repository copy of *Longitudinal dispersion affected by willow patches of low areal coverage*.

RESEARCH ARTICLE

WILEY

Longitudinal dispersion affected by willow patches of low areal coverage

Kaisa Västilä[1] | Jungsun Oh[2] | Fred Sonnenwald[3] | Un Ji[2,4] |
Juha Järvelä[1] | Inhyeok Bae[4] | Ian Guymer[3]

[1]Department of Built Environment, Aalto University School of Engineering, Espoo, Finland

[2]Department of Hydro Science and Engineering Research, Korea Institute of Civil Engineering and Building Technology, Goyang-Si, South Korea

[3]Department of Civil and Structural Engineering, University of Sheffield, Sheffield, UK

[4]Department of Civil and Environmental Engineering, University of Science and Technology, Goyang-Si, South Korea

Correspondence
Jungsun Oh, Department of Hydro Science and Engineering Research, Korea Institute of Civil Engineering and Building Technology, Goyang-Si, Korea.
Email: joh@kict.re.kr

Abstract

Vegetation notably influences transport and mixing processes and can thus be used for controlling the fate of substances in the hydro-environment. Whilst most work covers fully vegetated conditions, the novelty of this paper is to focus on flows with real-scale flexible willow patches. We aimed to investigate how longitudinal dispersion varies according to the spatial distribution, density and coverage of the patches and to evaluate the explanatory power of predictors that consider the hydraulics, vegetation and channel geometry. Salt tracer experiments were performed in a trapezoidal channel where we established 3–4 m long and 1–1.6 m wide patches of artificial foliated willows that reproduced the shapes and plant densities observed on woody-vegetated floodplains. We examined sparsely distributed patches with low areal/volumetric coverage of 6–11%, and non-vegetated conditions for reference. Flow depths and surface widths were 0.7–0.9 and 6–7 m, respectively, and the mean flow velocities ranged at 0.3–0.6 m/s. The emergent patches generated from a negligible to over a four-fold increase in the longitudinal dispersion when compared with non-vegetated conditions. The patches with a preferential location in low-velocity areas, such as near banks, or with a high plant density and a blockage of the cross-sectional flow area $\gtrsim 0.4$, led to the largest dispersion and residence times. Patches under such configurations enhanced the normalized differential velocity defined as the difference between the highest (90th percentile) and lowest (10th percentile) cross-sectional flow velocities divided by the mean velocity, thus increasing shear dispersion. As existing analytical predictors failed to estimate the effect of different patch configurations, we proposed the change in the normalized differential velocity between vegetated and corresponding non-vegetated conditions as a basic predictor of the reach-scale longitudinal dispersion coefficient under patchy vegetation. In contrast, we observed no clear relationship between flow resistance and dispersion. Thus, our findings indicated that bankside vegetation may allow for reduced peak concentrations and lengthened residence times, supporting pollutant management, while ensuring good flow conveyance. Such rare field-scale analyses improve the estimation of solute transport in real vegetated flows.

1 | INTRODUCTION

Vegetation significantly controls the mixing, transport and retention of soluble and particulate substances in the hydro-environment, influencing the fate of nutrients, suspended sediment and contaminants (e.g. Rowiński et al., 2018). Vegetated areas slow the flow and create regions with low or no flow, termed dead zones, which increase the transient storage and residence times in rivers, floodplains and wetlands (Murphy et al., 2007). By increasing the spread of substances, that is longitudinal dispersion, floodplain plants can reduce riverine peak concentrations during high flows or pollutant accidents (Hamidifar et al., 2015; Perucca et al., 2009). Once the substances have entered vegetated areas, they can be trapped within the sediment, taken up into the plant biomass or broken down, improving water quality (e.g. Västilä et al., 2021). Vegetation is thus a central part of nature-based solutions used in multifunctional river management (e.g. Jakubínský et al., 2021), but optimizing their performance requires an improved understanding of the underlying transport and mixing processes (Rowiński et al., 2021).

Vegetative effects on mixing have typically been quantified and modelled based on small-scale laboratory experiments with plants covering the entire channel bed (e.g. De Serio et al., 2018; Ghisalberti & Nepf, 2005; Sonnenwald et al., 2017). In reality, plants often do not grow as continuous stands but as distinct patches with marked edge effects (Figure 1; Larsen, 2019; Marion et al., 2014). Herein, we define the spatial plant arrangement with the patch matrix model describing the patchy vegetated reach as a mosaic of discretely delineated environmentally homogenous subunits (Hitchman et al., 2018; Lausch et al., 2015). Careful patch definition is particularly important in measuring and modelling, as different delineations are associated with different functions of the patches (Schoelynck et al., 2018). Vegetation patches can have areal coverages of 0–1

(Biggs et al., 2021; Verschoren et al., 2017; Yamasaki et al., 2019). A coverage of 0 represents an area devoid of vegetation, for example after hydraulic engineering works, vegetation maintenance or geomorphological events uprooting plants or burying vegetation (Wilcox & Shafroth, 2013). A coverage of 1 represents fully vegetated conditions. Herein, we consider vegetation coverages <0.2 as low and >0.5 as high.

The configuration and temporal dynamics of patches provide a useful template for a spatially explicit framework for river management (Erős & Lowe, 2019). In particular, plant patches could be favourable in human-impacted rivers requiring environmental improvements but disallowing natural recovery or full restoration because of flood management, irrigation and drainage, hydropower, recreational activities or disease control (González del Tánago et al., 2021; Thiemer et al., 2021). To support these human purposes, vegetation is currently widely removed from river and floodplain areas as part of routine maintenance, with the ecologically harmful complete removal through cutting still common (Rasmussen et al., 2021). As an alternative, maintaining patchy vegetation presents an intermediate solution between naturally vegetated and fully cut conditions and potentially allows optimizing between flow conveyance and water quality targets by influencing the flow resistance, dispersion, residence times and retention of soluble and particulate matter as analysed by Bal et al. (2011) and Verschoren et al. (2017) regarding aquatic plants. In addition, vegetation patches have been proposed as a mitigation measure against hydropeaking as they provide shelter for fish species during the rapid discharge changes generated by the operation of hydropower plants (Baladrón et al., 2021). Even relatively small patches can improve the ecological functioning of rivers and trigger further positive feedbacks, as found for aquatic vegetation (Licci et al., 2019).

Currently, there is a lack of validated predictors for estimating the influence of patchy vegetation on dispersion and residence times, and we are not aware of previous studies at real-scale focusing on the woody shrubs commonly found along rivers and floodplains. Of the few experiments with patchy vegetation, aquatic plants at high aerial coverages (>0.5) decreased dispersion (Verschoren et al., 2017) whereas patches of rigid cylinders at lower coverages increased dispersion compared with non-vegetated conditions (Park & Hwang, 2019). In addition, there are notable differences in the scaling of dispersion between patchy and fully vegetated conditions (Park & Hwang, 2019).

The most common approaches to modelling the transport and the associated temporal concentration distributions of solutes are the one-dimensional (1D) Advection–Diffusion Equation (ADE) based on the longitudinal dispersion coefficient D_x and the Aggregated Dead

FIGURE 1 Typical patch geometries of vegetation bars in Naesung stream of Korea: Sang-wol area located at 10 km upstream of the confluence with Nakdong River. Non-flood water level shown in light blue colour, vegetation patches formed of a mixture of willows and herbaceous plants in light yellow colour, dense and sparse herbaceous vegetation in green colour with dots and without dots, respectively, and sands in light grey colour

Zone Model (ADZ, e.g. Rutherford, 1994). The ADZ can describe the long recession tail of the temporal concentration distribution generated by transient storage, and yields the dispersive fraction D_f, characterizing the ratio of volume contributing to dispersion to total reach volume. In non-vegetated flows, D_x is commonly predicted based on channel width, depth, mean velocity and boundary shear velocity (e.g. Fischer, 1975; Wang & Huai, 2016). In fully vegetated flows, D_x is controlled by plant properties such as the density and drag coefficient, instead of the channel geometry (Lightbody & Nepf, 2006; Sonnenwald et al., 2019a).

Compared with non-vegetated and fully vegetated flows, the transport of solutes is more difficult to model under conditions where vegetation does not cover the entire flow area. Longitudinal dispersion is the bulk outcome of the shear dispersion generated by the spatial non-uniformity of the velocity distribution, turbulent diffusion facilitated by local turbulent velocity fluctuations, and transient storage (e.g. Boxall & Guymer, 2007), which are all influenced at several scales by plants (Marion et al., 2014; Shucksmith et al., 2011). For instance, patches modify the cross-sectional velocity distributions (Caroppi et al., 2022; Yamasaki et al., 2019) and generate turbulent fluctuations through the vortices at the lateral shear layers between each patch and open water and in the patch wake regions (e.g. Västilä et al., 2019). Smaller-scale turbulent fluctuations are caused by wake flows associated with stems and branches, dynamic movements of flexible leaves, and coherent motions of flexible interfaces (Caroppi & Järvelä, 2022).

For partly vegetated flows represented by rigid submerged vegetation (Murphy et al., 2007) or a compound channel with a fully vegetated floodplain (Huai et al., 2018), the mixing between vegetated and non-vegetated zones importantly controls the dispersion. Longitudinal dispersion in these scenarios can be calculated from the transverse variations of longitudinal velocity and eddy viscosity (Chikwendu, 1986). For patchy vegetation, the longitudinal dispersion is likely linked to several patch properties that modify the flow field, such as the plant density and flexibility (De Serio et al., 2018; Przyborowski et al., 2019) and the size and distribution of the patches (Barcelona et al., 2021; Luhar & Nepf, 2013). For clusters of cylinders, Park and Hwang (2019) proposed the clumpiness as a predictor of D_x but stated that future experiments are required to validate the findings to real-world conditions including complex flexible vegetation. Estimates based on direct concentration data are desirable as predictions based on hydrodynamic data only may substantially underestimate dispersion (Shin et al., 2020).

This contribution aims to 1) determine the variation in the longitudinal dispersion coefficient and dispersive fraction in a reach with real-scale flexible woody vegetation patches at different configurations, compared with non-vegetated conditions, 2) investigate how the plant density, coverage and spatial distribution of the patches control the flow field and thus the mechanisms contributing to dispersion and 3) evaluate the explanatory power of predictors that consider the hydraulic, vegetative and geometrical properties of the channel in estimating the influence of vegetation patches on reach-scale longitudinal dispersion. The scope of this paper is on sparsely distributed patches (6%–11% areal and volumetric coverage) and medium flow velocities typical for floodplains and channel margins (0.3–0.6 m/s).

2 | SITE AND METHODOLOGY

2.1 | Experimental channel with real-scale willow patches

An outdoor experiment channel at Korea Institute of Civil Engineering and Building Technology-River Experiment Center (KICT-REC) was used for controlled experiments with foliated vegetation patches. Experiments were conducted in a 78.8-m-long straight test section of a trapezoidal channel with a bottom width of 3 m, banks sloped at 1:2 and a bed slope of about 1/800 (Figure 2a). The banks were bare soil with scarce areas of low grasses and the bottom was movable sand.

Vegetation was introduced in the channel bottom by installing artificial foliated willows (details in Section 2.3) in eight equally spaced and sized patches in three different layouts aiming at reproducing the shapes of natural foliated floodplain willow patches (Figures 2b and 3). Based on the investigation of aerial photos for Naesung Stream, a tributary of Nakdong River near KICT-REC, most vegetation patches have a width-to-length ratio between 1:3 and 1:4 for single patches, with 2–3 patches clustered together (Figure 1). Such elongated patch shapes are typical across different hydro-environments (e.g. Larsen, 2019; Yamasaki et al., 2019). The sizes of the established patches fall to the lower range of values observed for riparian shrubs and low trees (Fernandes et al., 2011; Tagwireyi & Sullivan, 2015).

The experiments were conducted during campaigns in 2 years, both of which included four test cases with salt tracing (Table 1). In the labeling of the test cases, the first letter indicates the patch layout (A = alternating patches, B = bankside patches, C = centreline patches, NV = non-vegetated condition) and the second letter indicates the vegetation density measured through the patch leaf area index (see Section 2.3; D = dense, S = sparse). The last two letters distinguish the hydraulic boundary condition based on the cross-sectional mean flow velocity (LQ = low flow, MQ = medium flow, HQ = high flow).

The discharge was controlled by pumps and the downstream water level was regulated by a gate. The stability of the flow conditions was ensured with 2–3 ultrasonic sensors (HRXL-MaxSonar-WR, error 1%) installed both at the downstream bridge and in the upstream reservoir. Water depths were obtained from seven pressure sensors (OTT-PLS, error 0.05%) installed along the test section. The sensors were calibrated first under the same atmospheric pressure and second under the same hydrostatic pressure by temporally connecting them with piping. Water surface slope was calculated based on the sensors at cross-sections D2 and D14 (Figure 2a). Flow was close to uniform along the test section (Table 1). The cross-sectional geometry of sections D0, D2 and D14 was determined from total station surveys. Despite the establishment of bed forms during the experiments, the mean width and depth of the study reach remained reasonably constant for all examined cases.
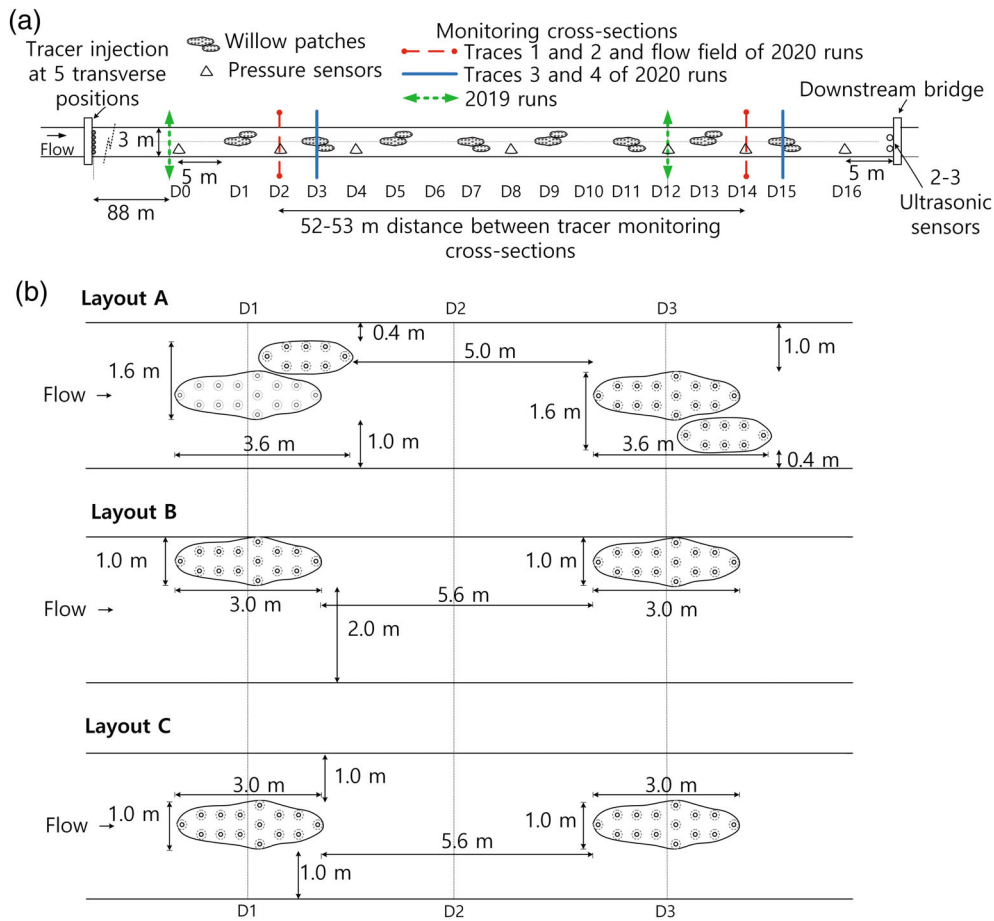
FIGURE 2 (a) Planform map of the experimental channel with the 8 willow patches and the measurement locations with respect to the 3-m-wide channel bed, and (b) the detailed patch layouts with the approximate edges of the foliated patches delineated while the circles denote the positions of the main stems of individual plants
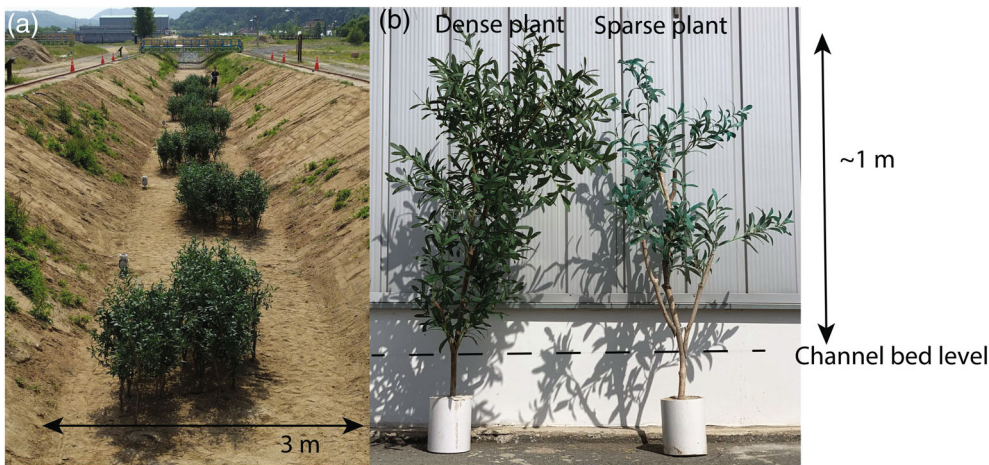
FIGURE 3 (a) Artificial willows installed in patches for the layout A, and (b) representative plants of the 2019 cases (sparse plant) and 2020 cases (dense plant)

2.2 | Determination of the discharge and flow velocity distribution

Flow velocities were measured using an acoustic doppler current profiler (ADCP, RiverSurveyor M9 by SonTek) at the D0 cross-section, 3.3 m upstream of the first patch, and in the 2020 cases additionally at D2 and D14 in the vegetated reach (Figure 2a). We applied the moving-boat method (Mueller et al., 2013), which measures slowly across from one side bank to another side bank several times. The data were collected and post-processed through the RiverSurveyor Live (RSL) by SonTek, and discharge was determined by averaging repeat measurement data. The methodology was validated in the same test channel by comparing to discharge over a wide-rectangular weir installed at the upstream reservoir, and the difference was approximately 4% (Bae & Ji, 2019).

TABLE 1 Hydraulic properties of the test cases

Test identifier (case no/year)	Label of the test case	Vegetation layout	Discharge (m^3/s)	Mean velocity u_m (m/s)	Water depth H (m)	Surface width (m)	Dry mass of salt (kg)	Number of EC sensors
01/2019	AS-HQ	A	2.81	0.62	0.94 (0.90–0.96)	6.44	1.0	2
02/2019	AS-MQ	A	1.95	0.51	0.83 (0.78–0.85)	6.08	3.5	2
03/2019	AS-LQ	A	1.49	0.44	0.75 (0.71–0.78)	5.82	5.0	2
07/2019	CS-LQ	C	1.47	0.44	0.73 (0.69–0.78)	5.76	3.4	2
01/2020	AD-LQ	A	1.44	0.34	0.82 (0.80–0.85)	6.46	3.5	6
05/2020	CD-LQ	C	1.49	0.34	0.83 (0.82–0.83)	6.58	3.5	6
09/2020	BD-LQ	B	1.47	0.33	0.84 (0.81–0.87)	6.71	3.5	6
13/2020	NV-LQ	NV	1.47	0.33	0.84 (0.83–0.84)	6.61	3.5	6

Notes: The vegetation layouts are illustrated in Figure 2b. For *H*, values are shown as the mean with the observed range in brackets.

TABLE 2 Vegetative properties for the different test cases

Label of the test case	$A_L/A_{B,P}$ (−)	$A_L/A_{B,R}$ (−)	$A_S/A_{B,P}$ (−)	$A_S/A_{B,R}$ (−)	A_L/V_P (1/m)	A_S/V_P (1/m)	ϕ_P (−)	ϕ_R (−)	V_P/V_W (−)	B_x (−)	I_P (−)
AS-HQ	2.6	0.39	0.38	0.058	2.7	0.41	0.0036	0.00054	0.10	0.40	0.15
AS-MQ	2.2	0.32	0.36	0.054	2.6	0.43	0.0038	0.00057	0.10	0.42	0.15
AS-LQ	1.9	0.28	0.32	0.049	2.5	0.43	0.0038	0.00038	0.10	0.43	0.15
CS-LQ	1.8	0.18	0.32	0.031	2.5	0.43	0.0038	0.00025	0.06	0.28	0.18
AD-LQ	4.9	0.91	0.34	0.064	6.0	0.42	0.0019	0.00021	0.11	0.40	0.15
CD-LQ	4.9	0.60	0.34	0.042	5.9	0.41	0.0019	0.00013	0.07	0.28	0.30
BD-LQ	4.2	0.61	0.30	0.043	5.1	0.35	0.0015	0.00013	0.08	0.30	0.30
NV-LQ	0	0	0	0	0	0	0	0	0	0	NA

Notes: Subscripts P and R refer to patch and reach scales, respectively, and subscripts L and S to properties for the foliage and stem, respectively.

To analyse the cross-sectional velocity distributions at D2 and D14, the local variability was reduced by spatially averaging the measured velocities using the velocity mapping toolbox (VMT by USGS, Parsons et al., 2013). To reduce the uncertainties due to the potential slight mis-orientation of the sensors, we adopted the velocity magnitude $U = \sqrt{u^2 + v^2 + w^2}$, where *u*, *v* and *w* are the flow velocities in the streamwise, lateral and vertical direction. The *U* values were manually extrapolated to the blank regions (Text S1), and the resulting discharges were within 10% of the discharges derived with the RSL, indicating that the manual extrapolation provided reasonable estimates of the near-boundary and near-surface velocities. We computed area-weighted cumulative probability distributions of *U* that were normalized by the cross-sectionally averaged *U* to remove the influence of the 10% uncertainty between the cases and cross-sections (Figure S1). The flow fields upstream of the vegetated area (cross-section D0) were comparable for similar discharges and water levels, as evidenced by the low between-cases differences in *U* (Figure S1) and in the cumulative probability distributions of the normalized *U* (Figure S2). Thus, the spatial variation in the velocities at D2 and D14 between the cases was ascribed to the changes in the vegetation properties.

2.3 | Properties of the artificial willow patches

The willows consisted of natural-growth willow stems with branches to which 0.30–0.40 m long foliated twigs made of plastic were attached so that the leaf area distribution in the foliage layer was approximately constant. We used similar branched stems in the 2019 and 2020 cases, but more foliated twigs were attached in the 2020 cases to mimic dense plants (Figure 3b). The main stem was cast in a concrete cylinder to anchor each willow securely in the channel bottom, and the stem was buried 30 cm below the channel bed level. Mean diameters of the main stem and branches were 23 and 15 mm, respectively, with the length-weighted mean diameter of the woody stems being 19 mm. The leaves were 75–90 mm long and 17–21 mm wide. The appearance of the artificial plants resembled *Salix subfragilis*, which is a native species to Korea, Japan, Russian Far East and northern China. The willows were emergent in all cases.

The key vegetative properties controlling the flow hydraulics were computed for the patch and reach scales based on a sample of 8–25 individual plants, considering the submerged plant parts only (Table 2). The patch scale considers the horizontal projection area of the canopy ($A_{B,P}$) obtained from terrestrial laser scanning (TLS) point

clouds. The reach-scale values take into account the total bed area in the investigated reach ($A_{B,R}$). Following the characterization of Västilä and Järvelä ([2018]), the foliage was described through the total one-sided leaf area (A_L) based on the area of individual leaves obtained through image analysis and the total number of leaves for the sample specimens. $A_L/A_{B,P}$ and $A_L/A_{B,R}$ refer to the patch-scale and reach-scale leaf area index (LAI), respectively. The total frontal stem area A_S consisting of the main stem, branches and twigs was calculated by multiplying the diameter of each element by its length. The LAI values are representative of natural woody vegetation (Antonarakis & Milan, [2020]).

The volumetric foliage and stem densities were computed as A_L/V_P and A_S/V_P where V_P is the water volume occupied by the patch ($V_P = A_{B,P}H$, H = water depth). The stem solid volume fractions (neglecting twigs) at the patch (ϕ_P) and reach scales (ϕ_R) were computed as the stem volume divided by V_P and V_W, respectively, where V_W is the total water volume in the reach. As the areal coverage is ambiguous to define in our channel due to the substantial gound area of the banks, we obtained the coverage as V_P/V_W, neglecting vertical variation in plant properties. The cross-sectional blockage factor B_x (Green, [2005]; Västilä & Järvelä, [2018]) was determined as the fraction of the wetted cross-section covered by the patch. To characterize the patchiness of the vegetation, we computed the standardized Morisita index I_P (Park & Hwang, [2019]; Smith-Gill, [1975]) using A_L as a measure of the vegetation density (see details in Text S2). I_P ranges from -1 to 1, with the higher values indicating a more spatially variable, or clumpier, vegetation cover.

2.4 | Salt tracing

For the present experiments, near-instantaneous injections of a salt tracer solution were applied following the concepts presented in Moore ([2005]). The tracer was poured from a bridge simultaneously at five positions across the channel (Figure [2]) to attain complete vertical and horizontal mixing before the upstream monitoring cross-section located 88–98 m downstream from the injection point. For the water depth H 1 m, complete vertical mixing was expected at around a 50 m distance based on the rough predictor $50H$ (Kalinowska, [2019]). The tracer solution was prepared by diluting a known amount of Korean sea salt (~85% NaCl) into channel water in a canister in a ratio of 1 kg to about 6 L, leading to the concentration of ~170 g/L. To evaluate the uncertainty of the measurements, four repeat traces were conducted for the 2020 cases.

The electric conductivity (EC) was measured at an upstream and downstream cross-section located at a constant 52–53 m longitudinal distance from each other, with six vegetation patches between them. The exact positions of the cross-sections were slightly different between the 2019 and 2020 cases (Figure [2]). For the 2019 cases, we monitored EC at mid-depth at the centreline of the non-vegetated cross-sections D0 and D12. For the 2020 cases, we monitored the non-vegetated cross-sections D2 and D14 for the repeat traces 1 and 2, and the vegetated cross-sections D3 and D15 for the repeat traces

3 and 4. In 2020, three EC sensors were located transversely at 0.25, 0.50 and 0.75 percentiles of the channel width at the mid-depth to improve the description of the cross-section.

For the 2019 cases, we used Omega CDH-SD1 EC sensors equipped with dataloggers sampling at 1 Hz. The sensors were set to auto-range for best accuracy. For 2020 cases, we used HOBO U24-001 Fresh Water Conductivity Data Logger recording at 1 Hz. The internal clocks of the sensors were automatically synchronized to the computer time before each run. The sensors were calibrated at different concentrations of the applied sea salt diluted into channel water in the 2019 runs and into distilled water in the 2020 runs. The sensors were rinsed in distilled water to remove any residual salt before taking each calibration reading. The sensors exhibited a very high linearity under all the calibration conditions, and the readings were within a 2.7% and 2.5% error range for the 2019 runs and 2020 runs, respectively (Figures S3 and S4).

The non-calibrated EC sensor data measured as electric conductivity (μS/cm) or concentration (ppm). Either was used for the analyses as the sensors had a linear response to concentration in mg/l. The sensor-measured background concentration was subtracted from the readings for the analyses. Data were mass-balanced (mass recovery ranged at 94%–105%, averaging 99%) as the ADE and ADZ analyses assume mass conservation and it improves the optimization. Data from 2020 runs at each of the three lateral downstream measurement positions were aligned by the t_{10} of the corresponding lateral location at the upstream cross-section, where t_{10} indicates the time at which 10% of the tracer mass has passed the sensor. The aligning removed the bias caused by the systematically faster arrival of the tracer at the right side of the upstream cross-section compared with the left side, which was presumably caused by a bend generating cross-sectional differences in flow upstream from the injection. The cross-sectional mean concentration was obtained through area-weighting of the data of the three lateral measurements.

2.5 | Estimating the parameters of Advection–Dispersion Equation and aggregate dead zone model

The parameters of the Advection–Dispersion Equation (ADE) and Aggregated Dead Zone Model (ADZ) were obtained by least-squares optimization of the prediction to the measured downstream concentration using MATLAB. The longitudinal dispersion coefficient D_x was derived from the ADE routing:

$$S(x_2,t) = \int_{\gamma=-\infty}^{\infty} \frac{S(x_1,\gamma)u_m}{\sqrt{4\pi D_x \bar{t}}} \exp\left[-\frac{u_m^2(\bar{t}-t+\gamma)^2}{4D_x\bar{t}}\right] d\gamma \quad (1)$$

where $S(x_1,t)$ is the observed upstream temporal concentration profile at time instant t, $S(x_2,t)$ is the observed downstream temporal concentration profile, u_m is the mean longitudinal velocity, $\bar{t}$ is the mean travel time and γ is a dummy variable of integration (Rutherford, [1994]).

The cell time constant α and the cell time delay τ were derived from the ADZ routing:

$$\widehat{S}^m = \exp(-\alpha\Delta t)S^{m-1} + (1 - \exp(-\alpha\Delta t))S_u^{m-\delta-1} \quad (2)$$

where S^m and S^{m-1} are concentrations at times $m\Delta t$ and $(m-1)\Delta t$, and $\delta = \text{floor}(\tau/\Delta t)$ with the floor function giving as output the greatest integer less than or equal to $\tau/\Delta t$ (Rutherford, 1994). We additionally calculated the travel time $\bar{t}_{ADZ} = \tau + 1/\alpha$ and the dispersive fraction $D_f = 1/(\alpha\bar{t}_{ADZ})$, which is the ratio of volume contributing to dispersion to total reach volume.

The goodness-of-fit R_t^2 was evaluated as:

$$R_t^2\left(S, \widehat{S}\right) = 1 - \frac{\sum_{k=1}^N \left(\widehat{S}_k - S_k\right)^2}{\sum_{k=1}^N S_k^2} \quad (3)$$

where $\widehat{S}_k$ is the predicted and S_k the measured kth concentration (Young et al., 1980).

We scaled the D_x and D_f values of the 2019 cases to ensure they are comparable to the spatially averaged 2020 values based on the three lateral measurement locations in two cross-sections (see Section 2.4). The scaling factors for each layout were determined from the 2020 data as the ratio between the spatially averaged value and the value obtained based on only the mid-channel sensors in the non-vegetated cross-section, the latter representing the measurement setting of the 2019 cases. The scaling factors were 1.19 for D_x (ratio of 0.71 ± 0.03 to 0.59 ± 0.15; mean $\mu \pm$ standard deviation σ), and 1.03 for D_f ($0.61 \pm 0.03 / 0.59 \pm 0.15$) for Layout A, and 0.70 for D_x ($0.35 \pm 0.02 / 0.50 \pm 0.07$) and 0.83 for D_f ($0.36 \pm 0.02 / 0.44 \pm 0.04$) for Layout C. The comparison between the mid-channel values in the non-vegetated cross-section and the spatially averaged values based on the measured (2020 cases) or the scaled (2019 cases) data (Figure S5) indicates that the scaling maintained the overall differences between the 2019 and 2020 cases and did not substantially alter the mean values of the different years.

2.6 | Predictors of D_x for non-vegetated, fully vegetated and patchy vegetated channels

Whilst a method for predicting dispersion in a reach with vegetation patches is lacking, we first compared the experimentally derived D_x with the methods proposed for non-vegetated and fully vegetated channels. Most of the models for non-vegetated channels are similar in formulation and accuracy, so we selected two widely applied models (Fischer, 1975; Wang & Huai, 2016). The experimental channel with limited bends and reasonably uniform cross-sections resembles the conditions under which these models were derived. Fischer (1975) gives:

$$D_x = \frac{0.011 u_m^2 B^2}{H u^*} \quad (4)$$

where u_m is mean flow velocity, B is channel width, H is water depth and u^* is the boundary shear velocity. Wang and Huai (2016) give

$$D_x = 0.0798 \left(\frac{B}{H}\right)^{0.6239} \left(\frac{u_m}{u^*}\right)^2 H u^* \quad (5)$$

The determination method of the basic variables u^* and B has a large influence on the predicted D_x in small vegetated channels with cross-sectionally non-uniform flow and banks forming a significant portion of the cross-section considering that there are uncertainties in the evaluation of u^* even in less complex conditions (Mrokowska & Rowiński, 2017). Therefore, we used two different definitions of u^* and B to understand their influence on the predictions under the patchy vegetated cases. First, we estimated u^* from $u^* = \sqrt{gHS_b}$, which assumes uniform flow in a wide unobstructed channel, where g is the acceleration due to gravity and S_b is channel bed slope, and second from $u^* = u_m/\sqrt{8/f}$ (Wang & Huai, 2016) which takes into consideration the total flow resistance relating Manning's n to the Darcy–Weisbach friction factor (f) determined as $f = 8gRS_w/u_m^2$ with the water surface slope S_w and hydraulic radius R. For B, we used the bed width, surface width and the mean width at the mid-depth.

D_x under fully vegetated flows with emergent plants of vertically uniform density can be predicted by Equation (6) (Lightbody & Nepf, 2006) and Equation (7) (Sonnenwald et al., 2019a):

$$D_x = 0.5 C_{D,S}^{1.5} u_m d \quad (6)$$

$$D_x = 0.6 u_m s_{50,P} \quad (7)$$

where d is the mean diameter of the stems. $C_{D,S}$ is the drag coefficient of the stem, and $C_{D,S} = 1$ was assumed representative under the examined velocities (Sonnenwald et al., 2019b) as the exact value of $C_{D,S}$ does not significantly impact the predicted D_x (Sonnenwald et al., 2018). $s_{50,P}$ is the patch-scale median stem spacing, which was estimated from ϕ_P and d according to Sonnenwald et al. (2019a). Herein, we extend Equation (7) to the reach scale by considering the reach-averaged median stem spacing $s_{50,R}$:

$$D_x = 0.6 u_m s_{50,R} \quad (8)$$

Equations (6)–(8) have been developed with $d < 2.54$ cm and $\phi_P < 0.05$, which conditions hold for the present dataset, and have been validated for rigid cylinders and herbaceous vegetation at $u_m < 0.1$ m/s (Lightbody & Nepf, 2006; Sonnenwald et al., 2019a). We acknowledge that the stem parameters neglect the influence of foliage (Aberle & Järvelä, 2013) but are not aware of formulas explicitly targeted for foliated vegetation, and thus Equations (6)–(8) are used to allow a rough comparison between fully and patchy vegetated flows.

In addition to Equations (4)–(8), we evaluated basic predictors that characterize the hydrodynamics and the main mechanisms expected to contribute to longitudinal dispersion in patchy vegetated flows. We considered the water surface slope, the standardized

Morisita index, f, and f/LAI, the latter representing well the specific flow resistance of foliated plants (e.g. Västilä & Järvelä, 2018). We propose U_{10} to describe the dead zone trapping effect, and the normalized differential velocity $U_d = (U_{90} - U_{10})/u_m$ in analogy to shear layer theory (e.g. Ho & Huerre, 1984) to characterize the differential advection and the associated shear dispersion, where U_{10} and U_{90} are the 10th and 90th percentile velocities of the area-weighted cumulative probability distributions of U (Section 2.2). Approximate estimates of U_d were derived for the 2019 cases lacking flow field data through scaling based on plant density and u_m (Text S3). We used cross-sections D2 and D14 to compare the cases; the reach-scale influence of patches was expected to be better captured at D14 with seven patches upstream, in comparison with D2 having only one patch upstream.

3 | RESULTS

3.1 | Influence of vegetation patches on velocity distributions

Comparison of the data downstream of the first (cross-section D2) and seventh (D14) of the eight patches indicated that the flow moderately developed in the downstream direction. This effect was greatest for the case with bankside patches (BD-LQ), whereas the cases with centreline patches (CD-LQ) and alternating patches (AD-LQ) showed less flow development (Figure 4; Figure S1). Hereafter, we will base our analyses on the data at D14, which is considered more representative of the conditions in the study reach.

Under the non-vegetated case, the central half of the wetted cross-section exhibited a constant $U \approx 0.4$ m/s, with lower values near the bed and on the banks (Figure 5). In the vegetated cases, U was reduced by ~50%–70% at the transverse locations downstream of the patches and increased at adjacent non-vegetated regions, with the

fastest local flow velocities of ~0.5 m/s observed for the alternating patches. The alternating (AD-LQ) and bankside (BD-LQ) patches reduced the lowest velocities, U_{10}, by 10%–14%, compared with the non-vegetated (NV-LQ) case, and increased the highest velocities, U_{90}, and the normalized differential velocity U_d by 20%–21% and 33%–36%, respectively (Table 3; Figure 4). In comparison, the centreline patches (CD-LQ) resulted in an approximately similar cumulative distribution of flow velocity as the non-vegetated case, increasing U_{90} and U_d by only 3%–4%.

3.2 | Optimized ADE and ADZ models

Both the ADE and ADZ approaches were satisfactorily fitted to all the runs, with each individual run showing $R_t^2 > 0.96$ for the ADE and $R_t^2 \geq 0.91$ for the ADZ. The variability between the repeat runs was low, with a coefficient of variability $c_v < 0.03$ for $u_{m,\text{ADE}}$, $\bar{t}_{\text{ADE}}$, $R_t^2{}_{,\text{ADE}}$, $u_{m,\text{ADZ}}$, $\bar{t}_{\text{ADZ}}$, and $R_t^2{}_{,\text{ADZ}}$. D_x and D_f exhibited $c_v < 0.11$ (averaging 0.07) for the vegetated cases, but higher values of $c_v = 0.12$–0.22 for the non-vegetated NV-LQ case. Subsequently, we use the mathematical means of the repeat runs for the 2020 cases (Table 4).

Across the investigated cases, the ADE predicted an early arrival of the plume and a late peak concentration (Figure 6). The ADE typically under-predicted concentrations during the latter half of the falling limb, except for the NV-LQ and CD-LQ cases, which had less skewed concentration distributions. The weakest ADE fit ($R_t^2 = 0.93$) was found for the BD-LQ case showing the most skewed downstream concentration profile, for which the ADE predicted a notably too early arrival of the plume and underestimated the long recession tail (Figure 6).

Predictions with the optimized parameters (Table 4) and a synthetic upstream concentration profile (a Gaussian distribution with $\bar{t} = 90$ s and $\sigma = 25$ s) indicated that the presence of vegetation patches decreased the downstream peak concentration compared with
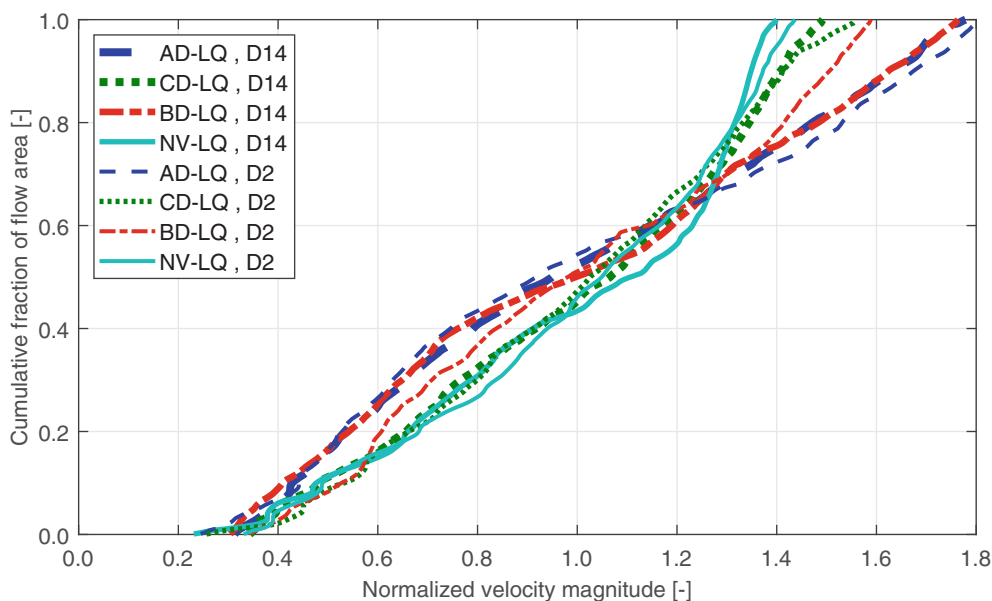

FIGURE 4 Comparison of cumulative distributions of normalized velocity magnitude along the vegetated reach (cross-sections D2 and D14) for the 2020 cases

FIGURE 5 Cross-sectional distributions of the velocity magnitude downstream of the seventh of the eighth vegetation patches (cross-section D14). The vertical green lines delineate the outer boundaries of the foliated vegetation patch located ~2 m upstream
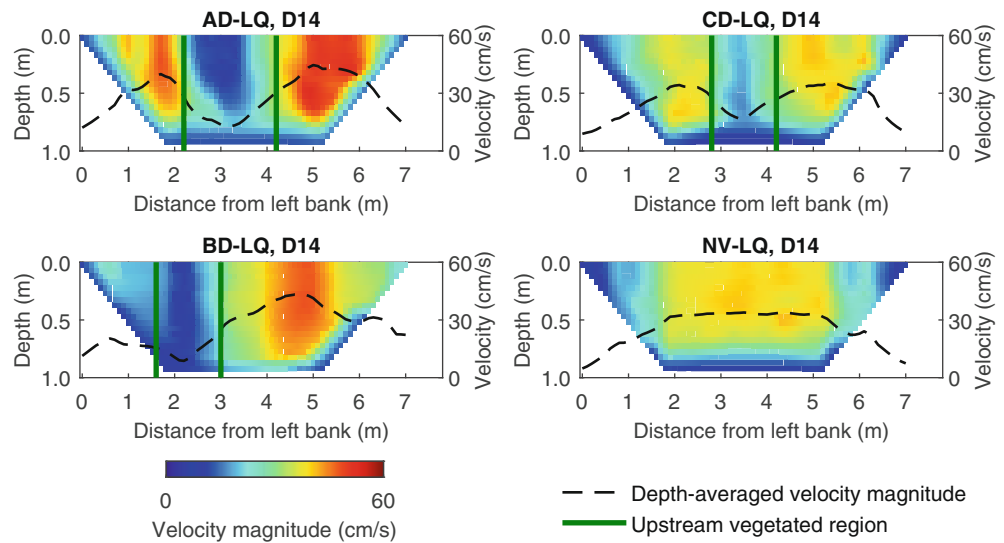

TABLE 3 Characteristic velocities (at D14) under the different cases

Case	U_{10} (m/s)	U_{90} (m/s)	U_d (m/s)
AS-HQ	NA	NA	0.87
AS-MQ	NA	NA	0.88
AS-LQ	NA	NA	0.89
CS-LQ	NA	NA	0.82
AD-LQ	0.13	0.50	1.09
CD-LQ	0.15	0.43	0.83
BD-LQ	0.12	0.49	1.11
NV-LQ	0.15	0.41	0.81

non-vegetated conditions, with the alternating and bankside patches leading to the largest decrease of ~40% (Figure 7). The patches increased the residence times as shown by the longer recession tails (Figure 7).

3.3 | Influence of the density and distribution of vegetation patches on longitudinal dispersion

To compare the test cases differing in upstream and downstream hydraulic boundary conditions, we used the commonly applied normalization $D_x/(u_mH)$ which satisfies the dimensionality (Wang & Huai, 2016). The normalization by u_mH was able to explain approximately half of the variation in D_x generated by the changing hydraulic forcing. This is shown by the data for the cases AS-HQ, AS-MQ and AS-LQ with equal patch geometry and density for which D_x increased by up to 74% with increasing u_m and H, while $D_x/(u_mH)$ decreased by 39%.

Figure 8 shows that all the three investigated vegetative characteristics—the density, coverage expressed as the ratio of the patch volume to total water volume (V_P/V_W), and spatial distribution

of the patches—influenced the dispersion, with very similar patterns observed for $D_x/(u_mH)$ and D_f. The alternating (layout A) and centreline (layout C) patches are grouped as centre patches for ease of interpretation, with $V_P/V_W = 0.06$–0.07 referring to layout C and $V_P/V_W = 0.10$–0.11 to layout A, and A exhibiting the higher $D_x/(u_mH)$ values. The largest effect was found for the spatial distribution of the patches, as demonstrated by the 2.4 units or 2.9 times higher $D_x/(u_mH)$ for the dense bankside patches (BD-LQ) than for the centreline patches with equal plant density and patch geometry (CD-LQ; purple non-filled arrow in Figure 8a). The dense patches resulted in a maximum of 2.8 units or 4.3 times higher $D_x/(u_mH)$ than the non-vegetated case (Figure 8a) whereas the influence of the sparse patches was notably lower, with a -0.2 to 0.3 units or -19% to 37% change in $D_x/(u_mH)$. $D_x/(u_mH)$ increased with increasing vegetation coverage, at a substantially greater rate for the denser patches (blue filled arrows in Figure 8a). As V_P/V_W was related to the cross-sectional blockage factor B_x by a multiplication factor of ~4 (Table 2), having B_x on the x axis of Figure 8 as B_x would lead to comparable trends. Finally, the ratio of volume contributing to dispersion to total reach volume (D_f) was ~3–9 times larger than the ratio of the patch volume to total water volume (V_P/V_W, Table 2, Figure 8b).

3.4 | Potential of selected hydrodynamic variables for predicting dispersion in a reach with vegetation patches

Equations (4) and (5) using mean width and u^* derived from the friction factor, as well as Equation (8), predicted a correct order of magnitude for D_x (Figures S6 and S7). However, none of these models were able to predict the increase in D_x generated by the dense vegetation patches, or the approximately threefold differences in D_x between the centreline and bankside patches of the same density and coverage. Similar predictive incapabilites were observed for the different definitions of B and u^*. The predictions with Equations (6) and (7) based on

TABLE 4 The optimized parameters and coefficients of determination for the ADE (Equation (1), subscript ADE) and the ADZ (Equation (2), subscript ADZ)

Case	$u_{m,ADE}$ (m/s)	$\bar{t}_{ADE}$ (s)	D_x (m²/s)	$R_t^2{}_{,ADE}$	$u_{m,ADZ}$ (m/s)	$\bar{t}_{ADZ}$ (s)	τ_{ADZ} (s)	D_f (—)	$R_t^2{}_{,ADZ}$
AS-HQ	0.467	109	0.49	0.990	0.443	115	89	0.24	0.985
AS-MQ	0.416	128	0.49	0.989	0.381	139	102	0.28	0.967
AS-LQ	0.348	153	0.28	0.989	0.327	163	128	0.22	0.985
CS-LQ	0.385	138	0.22	0.974	0.354	149	113	0.20	0.978
AD-LQ	0.307	168	0.71	0.988	0.275	188	117	0.61	0.979
CD-LQ	0.312	165	0.35	0.989	0.291	177	130	0.36	0.996
BD-LQ	0.336	154	1.02	0.930	0.288	179	103	0.74	0.986
NV-LQ	0.356	145	0.23	0.980	0.338	153	120	0.27	0.991

Notes: The values for the 2020 cases are averages between four repeat runs. Standard deviations are shown in Figure 8 for D_x and D_f while the other variables had appreciably lower σ/μ.
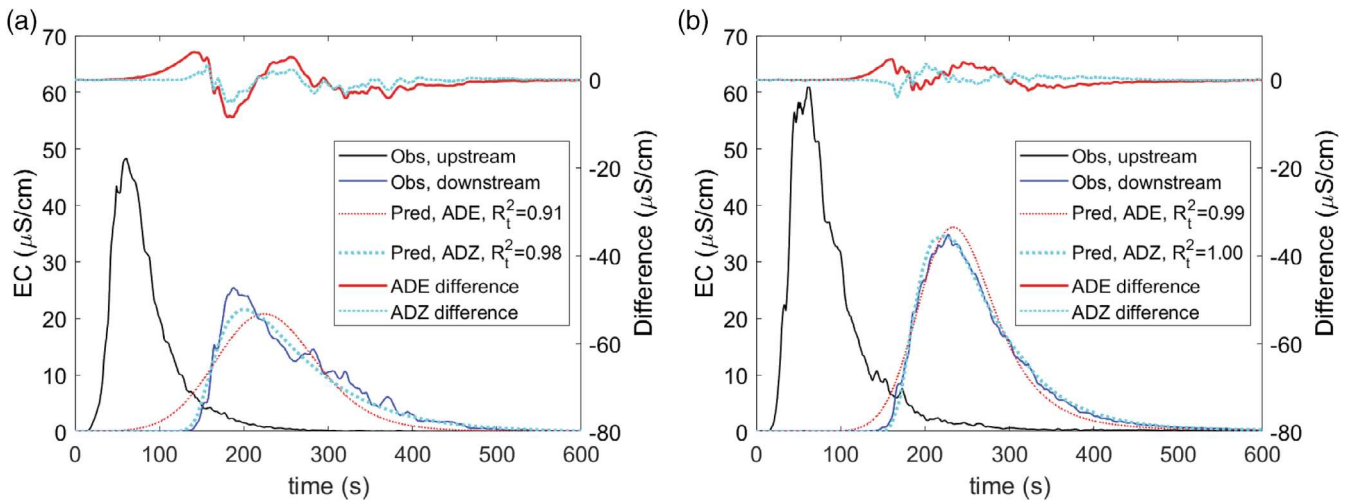
FIGURE 6 Observed and predicted concentrations for (a) the BD-LQ repeat run with the weakest ADE fit and (b) the CD-LQ repeat run with the overall best fits. The R_t^2 values of these particular runs differ slightly from the averaged values in Table 4

patch-scale vegetation properties were 1–2 orders of magnitude lower than the optimized values.

Of the examined predictors for patchy vegetation (see Section 2.6), neither the water surface slope (Figure 9a) nor the friction factor (Figure 9b) had a clear relationship with $D_x/(u_m H)$. Concerning the predictors applicable only to vegetated conditions, dispersion showed a weak negative relationship with the specific vegetative flow resistance (f/LAI) and a very weak dependence on the standardized Morisita index (Figure S8). Instead, a strong approximately linear regression was found between $D_x/(u_m H)$ and the normalized differential velocity U_d (Figure 9c), so that D_x under patchy vegetation could be estimated as

$$\frac{D_x}{u_m H} = \frac{D_{x,NV}}{u_{m,NV} H_{NV}} + \varepsilon(U_d - U_{d,NV}) \tag{9}$$

where the subscript NV represents the values in non-vegetated conditions and ε is a scaling factor for the influence of U_d, with

$U_{d,NV} = 0.81$ and $\varepsilon = 6.83$ under the presently examined conditions. The model predictions were substantially more accurate when using the tracer data for determining $D_{x,NV}$ (root mean squared errors RMSE of 0.91, Figure S9a) compared with estimating $D_{x,NV}$ from Equation (5) with the best-performing determination methods for u^* and B for the non-vegetated conditions ($u^* = \sqrt{gHS_b}$, B taken as bed width, RMSE of 0.50, Figure S9b).

4 | DISCUSSION

This work is novel in providing estimates of longitudinal dispersion in reaches with woody vegetation patches and linking those to the influence of the key patch properties on the hydrodynamics. Our tracer-based dispersion coefficients integrate the different contributing mechanisms, whereas many previous studies in vegetated flows use velocity-based D_x, which can be only one fourth or sixth of the concentration-based D_x (Shin et al., 2020). The skewed concentration

FIGURE 7 Synthetic upstream concentration profile normalized by the peak concentration, and predictions for the downstream cross-section at 53 m distance using optimized model parameters of the (a) ADE and (b) ADZ for the 2020 cases. 2019 cases were left out for clarity but had approximately similar concentration profiles as NV-LQ
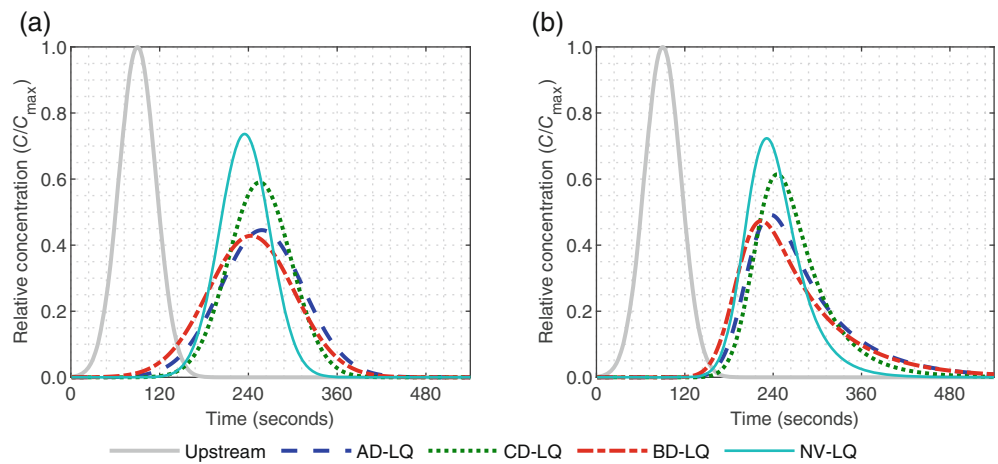

FIGURE 8 Influence of coverage (V_P/V_W), plant density (sparse vs dense), and spatial distribution (centre vs bankside) of the patches on (a) normalized longitudinal dispersion $D_x/(u_mH)$ and (b) dispersive fraction D_f. Error bars denote the standard deviation for the cases with repeat runs. V_P/V_W can be approximately translated to the cross-sectional blockage factor B_x by multiplying by 4 (Table 2).
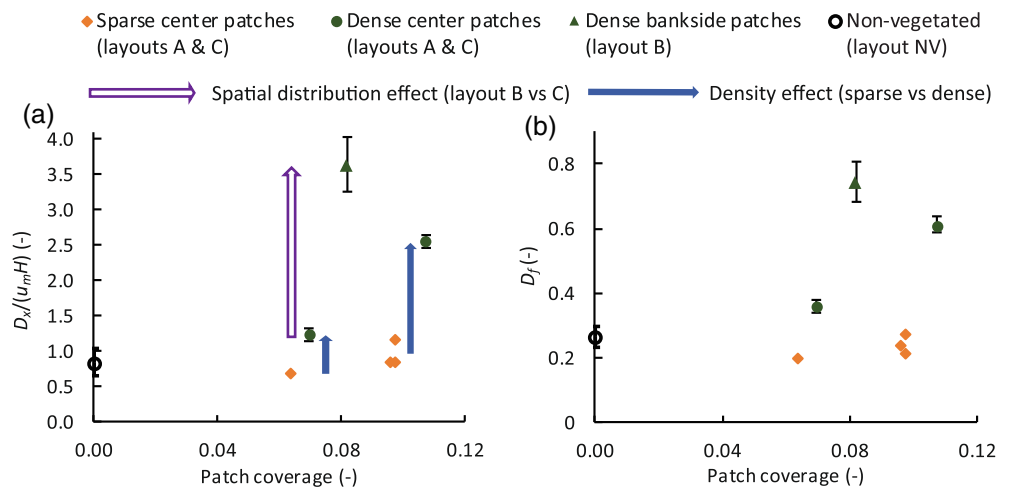
distributions (Figure 6) indicated that the experiments covered non-equilibrium conditions with non-complete horizontal mixing (e.g. Shucksmith et al., 2007), under which the 1D ADE model is not fully valid. However, the 1D model is commonly applied despite such violations in the assumptions as estimates of the four components of the 2D dispersion tensor are typically unavailable (e.g. Kalinowska, 2019). In fact, complete mixing cannot be realistically expected for the bankside patches. Nevertheless, the obtained D_x values may be used for comparing the different cases, which was the primary focus of this study.

4.1 | Potential implications of vegetation patches on riverine transport processes

The present results can help in using patchy vegetation to control the transport and fate of harmful substances (e.g. Rowiński et al., 2021). Sparsely distributed patches with a coverage (V_P/V_W) of 6%–11% can cause from a negligible to 4.3-fold increase in dispersion compared with non-vegetated conditions (Figure 8). As V_P/V_W was linearly

related to the cross-sectional blockage factor (B_x, Table 2), Figure 8 suggests that allowing or establishing dense woody patches in low-velocity areas or so that they cover ≳40% of the flow area in the cross-section increases the residence times, enhancing the potential for substances to be retained or processed into less harmful compounds. The results implied that even relatively small woody patches, in our case of 3–4 m length and 1–2 m width, are sufficient to reach such effects while a threshold length of 0.3–1 m for sediment accumulation has been reported for aquatic patches (Licci et al., 2019). For water quality benefits, woody patches with a typically several times lower volumetric plant density (A_L/V_P ~ 2.5–6, Table 2) likely need to be larger than aquatic patches with A_L/V_P up to ~100 (Luhar & Nepf, 2013).

Regarding multifunctional management of rivers optimizing between flow conveyance and environmental targets, we did not observe a general relationship between reach-scale flow resistance and dispersion (Figure 9b). In fact, patches located near to the banks created notably longer residence times than channel centre patches and non-vegetated conditions, while their flow resistance was substantially lower than for the centre patches and only slightly higher
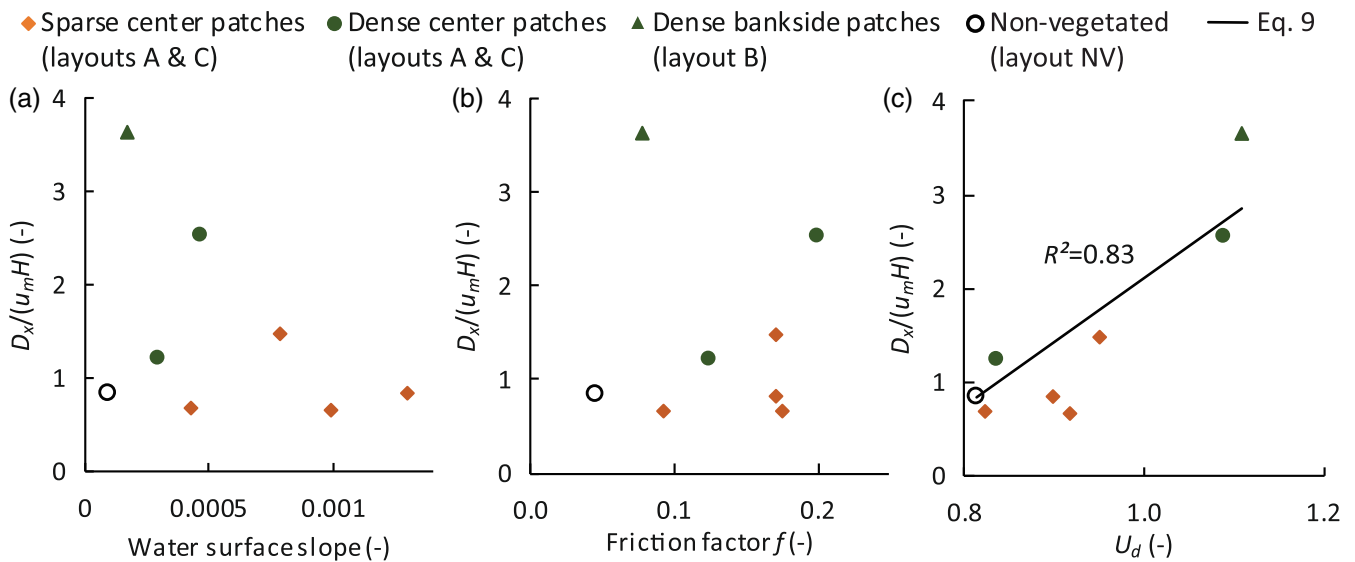
FIGURE 9 Normalized dispersion as a function of (a) water surface slope, (b) friction factor and (c) normalized differential velocity, with the line showing the prediction according to Equation (9)

than for the non-vegetated conditions. Thus, leaving vegetation on channel margins while cutting it from the channel centre, as also proposed by Errico et al. (2019), provides a potential scenario for environmentally preferable vegetation management as an alternative to the common complete vegetation cut to ensure flow conveyance (Bączyk et al., 2018; Biggs et al., 2021). These implications cannot be directly extended to mean velocities other than the examined range of ~0.3–0.4 m/s as the influence of u_m on the modification of flow resistance and hydrodynamics at the patch mosaic scale is not fully clear (see also Barcelona et al., 2021; Licci et al., 2019).

4.2 | The influence of plant patches on dispersion differs from non-vegetated and fully vegetated conditions

The low-coverage patches resulted in a maximum of three times larger impact on reach-scale dispersion than homogeneous vegetation on floodplains, which can increase D_x of compound channels by 1.5-fold (Perucca et al., 2009). In addition, the highest dispersive fractions of our patchy vegetation were larger than reported for randomly distributed woody stems at notably lower flow velocities (D_f = 0.2–0.5; Carling et al., 2020).

Our results demonstrate that patchy vegetation influences dispersion markedly differently than uniformly distributed vegetation. The comparison of the methods for non-vegetated (Equations (4) and (5)) and fully vegetated (Equations (6) and (7)) flows indicates that full vegetation coverage reduces D_x by 1–2 orders of magnitude, whereas patchy vegetation increases dispersion (Figure S6). This finding agrees with the laboratory experiments of Park and Hwang (2019) under comparable low coverages who observed that D_x in vegetated conditions is larger than in the non-vegetated case and increases steeply as

vegetation is organized into more distinct groups. While Equations (4), (5), (8) yielded a correct order of magnitude for D_x, they did not capture the tendency of the vegetation patches to increase D_x. Equations (4) and (5) assume that D_x is inversely proportional to u^* but both D_x and u^* derived from the friction factor rose in the presence of patches. In addition, Equations (4) and (5) as well as Rutherford (1994, figure 4.8 on p. 200) and Zeng and Huai (2014) suggest that D_x declines with decreasing width-to-depth ratio (B/H). In contrast, considering only the non-vegetated areas, patchy vegetation decreased B/H while augmenting D_x. We expect these changes in the geometry of the unobstructed flow area due to vegetation to have some effect on D_x, but additional data are required for more detailed analyses.

Of the other examined predictors, the friction factor normalized by the leaf area index (f/LAI, Figure S8) provided weaker explanatory power than a comparable measure of the specific vegetative drag, drag coefficient, for patches of rigid cylinders (Park & Hwang, 2019). For our highly clumpy vegetation (I_P of 0.15–0.30, Table 2), the standardized Morisita index I_P had a noticeably poorer predictive power than under the less clumped conditions of Park and Hwang (2019) with 1–3 orders of magnitude lower I_P, indicating that the plant density and the patch location in the cross-section importantly control dispersion in addition to the clumpiness.

4.3 | Differential velocity allows estimating longitudinal dispersion in a reach with vegetation patches

Longitudinal dispersion in a reach with emergent vegetation patches was most reliably explained by the strength of the cross-sectional variability of the flow velocity, expressed through the normalized differential velocity $U_d = (U_{90} - U_{10})/u_m$ (Figure 9c). The mixture of

vegetated regions with low velocities and non-vegetated regions with high velocities significantly increases the non-uniformity of velocity and thus D_x compared with fully vegetated channels (e.g. Yamasaki et al., 2019, Figure S6). Even changes of ~10%–20% in the highest and lowest cross-sectional velocities (Table 3) significantly increased D_x, reinforcing that reach-averaged bulk hydraulic parameters cannot predict how different patch configurations, such as plant density, coverage and spatial distribution of the patches, influence the reach-scale dispersion (Figure 9a,b, Figures S6–S8). The influence of U_d was incorporated into Equation (9), which Figure 9c showed to allow estimating D_x under patchy vegetation at low coverages while further validation is required to define the upper limit of vegetation coverage.

The mean velocities and water depths under non-vegetated and patchy vegetated conditions ($u_{m,NV}$, u_m, H_{NV} and H) required by Equation (9) can be obtained from measurements of the cross-sectional flow area and discharge, or from standard 1D hydraulic modelling. As an alternative to modelling of the vegetated conditions, a rough estimate for low-coverage woody patches can be obtained based on Table 1: the mean velocities can be assumed to be slightly decreased and water depths slightly increased compared to the non-vegetated conditions with similar discharge and downstream water level. The most reliable estimates of $D_{x,NV}$ can be obtained from tracer tests if vegetation is cut, for example from a short reference reach (see also Figure S9). Alternatively, $D_{x,NV}$ can be obtained, for example based on Equations (4) and (5) or some of the other numerous predictors for unobstructed channels (e.g. Wang & Huai, 2016; Zeng & Huai, 2014) although further work focusing on optimizing predictors of $D_{x,NV}$ for small channels is recommended. In our small channel with a low width-to-depth ratio of <8, Equation (5) provided more reliable $D_{x,NV}$ estimate than Equation (4) (Figure S7), which agrees with the reported under-estimation of Equation 4 for natural channels with $B/H < 20$ (Zeng & Huai, 2014). If a reliable estimate of $D_{x,NV}$ cannot be feasibly obtained, Equation 9 can be used to estimate the relative influence of the patches, that is for comparing the normalized dispersion under non-vegetated ($D_{x,NV}/(u_{m,NV}H_{NV})$) and patchy vegetated ($D_x/(u_m H)$) flows.

Accurate estimates of $U_{d,NV}$ and $U_{d,}$ require measurements or models of the mean velocity distribution. For emergent vegetation under field conditions where a 3D spatial distribution of the flow is unfeasible to obtain, we recommend focusing on the transverse variability in flow velocity, for example through depth-averaged numerical or analytical models which are readily available (e.g. Dalledonne et al., 2019; Tang & Knight, 2009). The vertical variability in velocity is generally low even within complex vegetation (Figure 5, Xu & Nepf, 2020). In addition, most species prefer certain flow velocity and water depth ranges (e.g. O'Hare et al., 2016), and such non-random positioning in the cross-section limits the longitudinal flow variability. For example, patch widths as low as 1–2 m create wake flows extending up to tens of meters, so that the velocity does not fully recover between the patches (e.g. Caroppi et al., 2022; Marjoribanks et al., 2019). The uncertainty in modelling the mean velocity distributions in partly vegetated flows (e.g. Kiczko et al., 2020) is expected to improve in the future as more advanced parameterizations of

vegetation are being incorporated into numerical models (Box et al., 2021). Finally, further investigations are recommended under different patch configurations and channel boundary conditions to evaluate ε.

4.4 | Mechanisms contributing to dispersion under different patch configurations

Dead zone trapping generated by the patches was modest in most cases, with concentrations rapidly decreasing to the background level (Figure 6) and even the dense patches having a limited effect on the lowest velocities (Table 3). By contrast, the larger increases in U_{90} and particularly U_d indicated that shear dispersion was the main mechanism contributing to higher D_x in the presence of patches. While all riverine patches generally reduce the local streamwise velocities (Figure 5; Västilä et al., 2019), sparse or low blockage ($B_x \lessgtr 0.3$) patches situated in the central part of the cross-sections increased velocities close to banks, thus generating only slightly higher differential advection compared with non-vegetated conditions. By contrast, patches located particularly in low-velocity regions, such as near the banks, accentuated the cross-sectional velocity variability, hence enhancing dispersion. Our case with the bankside patches leaving the upper part of the bank unvegetated (layout B) likely slightly increased dispersion compared to the more commonly observed case of vegetation extending over the entire bank. However, the bank region had nearly uniform and notably lower velocities than in the non-vegetated case (Figure 5), contributing comparatively little to the shear dispersion as opposed to the substantial additional shear over the channel centre and other bank.

The increase in D_f of 0.3–0.5 for the alternating and bankside patches with coverages of 6%–11% indicated that not only the vegetated areas but also the areas between longitudinally subsequent patches, characterized by wake flows, contributed to dispersion. For the bankside patches, dispersion and trapping were likely augmented by the slow flow area extending down to the channel bed (Figure 5) and by the consistent lateral positioning of the patches, both expected to decrease the cross-sectional mixing. In contrast, the alternating patches diverting the flow towards the downstream non-vegetated bank likely enhanced mixing, which presumably moderated their influence on D_x.

The sparse or low-coverage central patches with had a less important influence on the dispersion compared to the channel boundaries, bedforms, and sparse patches of low grasses on the banks (Figure 3a), as indicated by the only slightly larger D_x and D_f values compared with non-vegetated condition (Figure 8). The dominance of boundary effects is typical in such small channels with a large wetted perimeter in relation to the flow area (e.g. Ensign & Doyle, 2006). D_f of the non-vegetated condition was deemed representative of natural rivers, with over 90% of UK rivers having $D_f = 0$–0.35 (Guymer, 2002), but was higher than the UK average of $D_f = 0.15$–0.2 likely because of the substantial-sized bedforms observed on the sandy bed in comparison with UK rivers exhibiting typically finer substrates and lower flow velocities.

4.5 | Benefits and limitations of the experimental methodology

The acceptable uncertainty (Figure 8) indicated that the 2020 measurement design based on three laterally distributed mid-depth sensors was well suited for such small channels (width < 10 m) with emergent plant patches. The mean σ was 76% lower when measuring at three lateral locations ($\sigma = 0.05$) compared with measuring only at the centre of the cross-section ($\sigma = 0.22$). The average values were fairly similar with -20% to 30% differences. Thus, the reliability of concentration and D_x values in channels with plant patches can be notably improved by simultaneous measurements at several locations in the cross-section characterized by different flow velocities, or by averaging the results over multiple runs if few sensors are available. We recognize that our 2019 data have more uncertainty compared with the 2020 data as the 2019 values were based on only mid-channel sensors with no repeated measurements (Section 2.4). Despite scaling the 2019 data to be comparable with the 2020 data (Section 2.5), there is a higher uncertainty in comparing the cases between the different years as opposed to analysing the between-cases differences separately for the 2019 and 2020 datasets. If regarded independently, both datasets show the same trends and approximately similar regression slopes (Figure 9c), supporting the main finding that U_d is the key controlling factor on dispersion under patchy vegetation.

We acknowledge that our data covers a limited range of conditions but expect that the results can be extended to slightly outside the studied ranges of flow velocity, plant density and coverage. The study setting lacking grassy understory likely under-estimates D_x for the commonly observed case with grasses growing below the foliage zone of woody shrubs (Berends et al., 2020; Carling et al., 2020). It would be beneficial to complement the dataset with mean velocities <0.3 m/s typical for lowland channels and floodplains with more pronounced transient storage, and with rarely investigated patch coverages of ~20%–50%. Experiments focusing on the mixing between open water and woody patches would enhance understanding of the processes impacting the reach-scale bulk dispersion and retention.

5 | CONCLUSIONS

Our field-scale investigations with realistic artificial vegetation have improved understanding of how plant patches control the transport of solutes in river and floodplain flows. Specifically, our work is novel in determining concentration-based estimates of the longitudinal dispersion coefficient (D_x) and the dispersive fraction (D_f) for flexible woody vegetation at the patch mosaic scale. The sparsely distributed emergent patches with areal/volumetric coverages of 6%–11% were found to create from a negligible to over fourfold increase in reach-scale dispersion compared to non-vegetated conditions. Thus, patchy vegetation was shown to have an opposite influence on D_x than the commonly investigated case of full vegetation coverage, which

decreases dispersion. The highest dispersion was found for the dense patches having a cross-sectional blockage $\gtrsim 40\%$ or located in low-velocity areas, such as preferentially along the bankside. The results indicate that shear dispersion through enhanced differential advection is the main mechanism increasing the reach-scale D_x and D_f under patchy vegetation. The most pronounced transient storage was exhibited by the bankside vegetation. The influence of patch density, coverage and spatial distribution on reach-scale dispersion cannot be reliably predicted using the widely applied analytical models for open channel flows (e.g. Equations (4) and (5)), because they do not describe the changes in the differential advection. Thus, we proposed Equation (9) with the normalized differential velocity $U_d = (U_{90} - U_{10})/u_m$ as a basic estimator for D_x under patchy vegetated flows. From the river management viewpoint, bank vegetation was found to provide notably lower flow resistance but higher dispersion and longer residence times than channel centre vegetation of the same density and coverage. Thus, maintaining vegetation in channel margins may enable the trapping and processing of nutrients and harmful substances while ensuring acceptable water levels during high flows, but further validation is needed outside of the presently examined velocity range.

DATA AVAILABILITY STATEMENT

The data that support the findings of this study are available from the corresponding author upon reasonable request.

ORCID

Kaisa Västilä https://orcid.org/0000-0002-6034-760X
Fred Sonnenwald https://orcid.org/0000-0002-2822-0406
Juha Järvelä https://orcid.org/0000-0001-7499-8414
Ian Guymer https://orcid.org/0000-0002-1425-5093

REFERENCES

Aberle, J., & Järvelä, J. (2013). Flow resistance of emergent rigid and flexible floodplain vegetation. *Journal of Hydraulic Research*, *51*(1), 33–45. https://doi.org/10.1080/00221686.2012.754795

Antonarakis, A. S., & Milan, D. J. (2020). Uncertainty in parameterizing floodplain Forest friction for natural flood management, using remote sensing. *Remote Sensing*, *12*(11), 1799. https://doi.org/10.3390/rs12111799

Bączyk, A., Wagner, M., Okruszko, T., & Grygoruk, M. (2018). Influence of technical maintenance measures on ecological status of agricultural lowland rivers—Systematic review and implications for river management. *The Science of the Total Environment*, *627*, 189–199. https://doi.org/10.1016/j.scitotenv.2018.01.235

Bae, I., & Ji, U. (2019). Outlier detection and smoothing process for water level data measured by ultrasonic sensor in stream flows. *Water*, *11*(5), 951. https://doi.org/10.3390/w11050951

Bal, K., Struyf, E., Vereecken, H., Viaene, P., De Doncker, L., de Deckere, E., Mostaert, F., & Meire, P. (2011). How do macrophyte distribution patterns affect hydraulic resistances? *Ecological Engineering*, *37*(3), 529–533. https://doi.org/10.1016/j.ecoleng.2010.12.018

Barcelona, A., Oldham, C., Colomer, J., & Serra, T. (2021). Functional dynamics of vegetated model patches: The minimum patch size effect for canopy restoration. *Science of the Total Environment*, *795*, 148854. https://doi.org/10.1016/j.scitotenv.2021.148854

Berends, K. D., Ji, U., (Ellis) Penning, W. E., Warmink, J. J., Kang, J., & Hulscher, S. J. M. H. (2020). Stream-scale flow experiment reveals large influence of understory growth on vegetation roughness. *Advances in Water Resources*, *143*, 103675. https://doi.org/10.1016/j.advwatres.2020.103675

Biggs, H. J., Haddadchi, A., & Hicks, D. M. (2021). Interactions between aquatic vegetation, hydraulics and fine sediment: A case study in the Halswell River, New Zealand. *Hydrological Processes*, *35*(6), e14245. https://doi.org/10.1002/hyp.14245

Box, W., Järvelä, J., & Västilä, K. (2021). Flow resistance of floodplain vegetation mixtures for modelling river flows. *Journal of Hydrology*, *601*, 126593. https://doi.org/10.1016/j.jhydrol.2021.126593

Boxall, J. B., & Guymer, I. (2007). Longitudinal mixing in meandering channels: New experimental data set and verification of a predictive technique. *Water Research*, *41*(2), 341–354. https://doi.org/10.1016/j.watres.2006.10.010

Carling, P. A., Leyland, J., Kleinhans, M. G., Besozzi, L., Duranton, P., Trieu, H., & Teske, R. (2020). Quantifying fluid retention due to natural vegetation in a Forest floodplain analogue using the aggregated dead zone (ADZ) dilution approach. *Water Resources Research*, *56*(9), e2020WR027070. https://doi.org/10.1029/2020WR027070

Caroppi, G., & Järvelä, J. (2022). Shear layer over floodplain vegetation with a view on bending and streamlining effects. *Environmental Fluid Mechanics*, 1–32. https://doi.org/10.1007/s10652-022-09841-w

Caroppi, G., Västilä, K., Järvelä, J., Lee, C., Ji, U., Kim, H. S., & Kim, S. (2022). Flow and wake characteristics associated with riparian vegetation patches: Results from field-scale experiments. *Hydrological Processes*, *36*(2), e14506. https://doi.org/10.1002/hyp.14506

Chikwendu, S. C. (1986). Application of a slow-zone model to contaminant dispersion in laminar shear flows. *International Journal of Engineering Science*, *24*(6), 1031–1044. https://doi.org/10.1016/0020-7225(86)90034-0

Dalledonne, G. L., Kopmann, R., & Brudy-Zippelius, T. (2019). Uncertainty quantification of floodplain friction in hydrodynamic models. *Hydrology and Earth System Sciences*, *23*(8), 3373–3385. https://doi.org/10.5194/hess-23-3373-2019

De Serio, F., Ben Meftah, M., Mossa, M., & Termini, D. (2018). Experimental investigation on dispersion mechanisms in rigid and flexible vegetated beds. *Advances in Water Resources*, *120*, 98–113. https://doi.org/10.1016/j.advwatres.2017.08.005

Ensign, S. H., & Doyle, M. W. (2006). Nutrient spiraling in streams and river networks. *Journal of Geophysical Research – Biogeosciences*, *111*(G4), 1–13. https://doi.org/10.1029/2005JG000114

Erős, T., & Lowe, W. H. (2019). The landscape ecology of Rivers: From patch-based to spatial network analyses. *Current Landscape Ecology Reports*, *4*(4), 103–112. https://doi.org/10.1007/s40823-019-00044-6

Errico, A., Lama, G. F. C., Francalanci, S., Chirico, G. B., Solari, L., & Preti, F. (2019). Flow dynamics and turbulence patterns in a drainage channel colonized by common reed (Phragmites australis) under different scenarios of vegetation management. *Ecological Engineering*, *133*, 39–52. https://doi.org/10.1016/j.ecoleng.2019.04.016

Fernandes, M. R., Aguiar, F. C., & Ferreira, M. T. (2011). Assessing riparian vegetation structure and the influence of land use using landscape metrics and geostatistical tools. *Landscape and Urban Planning*, *99*(2), 166–177. https://doi.org/10.1016/j.landurbplan.2010.11.001

Fischer, H. B. (1975). Discussion of 'simple method for predicting dispersion in streams' by R.S. McQuivey and T.N. Keefer. *Journal of Environmental Engineering*, *101*(3), 453–455. https://doi.org/10.1061/JEEGAV.0000360

Ghisalberti, M., & Nepf, H. (2005). Mass transport in vegetated shear flows. *Environmental Fluid Mechanics*, *5*(6), 527–551. https://doi.org/10.1007/s10652-005-0419-1

González del Tánago, M., Martínez-Fernández, V., Aguiar, F. C., Bertoldi, W., Dufour, S., García de Jalón, D., Garófano-Gómez, V., Mandzukovski, D., & Rodríguez-González, P. M. (2021). Improving river hydromorphological assessment through better integration of riparian vegetation: Scientific evidence and guidelines. *Journal of Environmental Management*, *292*, 112730. https://doi.org/10.1016/j.jenvman.2021.112730

Green, J. C. (2005). Comparison of blockage factors in modelling the resistance of channels containing submerged macrophytes. *River Research and Applications*, *21*(6), 671–686. https://doi.org/10.1002/rra.854

Guymer, I. (2002). A national database of travel time, dispersion and methodologies for the protection of river abstractions. Environment Agency R & D Technical Report P346.

Hamidifar, H., Omid, M. H., & Keshavarzi, A. (2015). Longitudinal dispersion in waterways with vegetated floodplain. *Ecological Engineering*, *84*, 398–407. https://doi.org/10.1016/j.ecoleng.2015.09.048

Hitchman, S. M., Mather, M. E., Smith, J. M., & Fencl, J. S. (2018). Identifying keystone habitats with a mosaic approach can improve biodiversity conservation in disturbed ecosystems. *Global Change Biology*, *24*(1), 308–321. https://doi.org/10.1111/gcb.13846

Ho, C., & Huerre, P. (1984). Perturbed free shear layers. *Annual Review of Fluid Mechanics*, *16*, 365–422. https://doi.org/10.1146/annurev.fl.16.010184.002053

Huai, W., Shi, H., Song, S., & Ni, S. (2018). A simplified method for estimating the longitudinal dispersion coefficient in ecological channels with vegetation. *Ecological Indicators*, *92*, 91–98. https://doi.org/10.1016/j.ecolind.2017.05.015

Jakubínský, J., Prokopová, M., Raška, P., Salvati, L., Bezak, N., Cudlín, O., Cudlín, P., Purkyt, J., Vezza, P., Camporeale, C., Daněk, J., Pástor, M., & Lepeška, T. (2021). Managing floodplains using nature-based solutions to support multiple ecosystem functions and services. *WIREs Water*, *8*(5), e1545. https://doi.org/10.1002/wat2.1545

Kalinowska, M. B. (2019). Effect of water–air heat transfer on the spread of thermal pollution in rivers. *Acta Geophysica*, *67*(2), 597–619. https://doi.org/10.1007/s11600-019-00252-y

Kiczko, A., Västilä, K., Kozioł, A., Kubrak, J., Kubrak, E., & Krukowski, M. (2020). Predicting discharge capacity of vegetated compound channels: Uncertainty and identifiability of one-dimensional process-based models. *Hydrology and Earth System Sciences*, *24*(8), 4135–4167. https://doi.org/10.5194/hess-24-4135-2020

Larsen, L. G. (2019). Multiscale flow-vegetation-sediment feedbacks in low-gradient landscapes. *Geomorphology*, *334*, 165–193. https://doi.org/10.1016/j.geomorph.2019.03.009

Lausch, A., Blaschke, T., Haase, D., Herzog, F., Syrbe, R.-U., Tischendorf, L., & Walz, U. (2015). Understanding and quantifying landscape structure – A review on relevant process characteristics, data models and landscape metrics. *Ecological Modelling*, *295*, 31–41. https://doi.org/10.1016/j.ecolmodel.2014.08.018

Licci, S., Nepf, H., Delolme, C., Marmonier, P., Bouma, T. J., & Puijalon, S. (2019). The role of patch size in ecosystem engineering capacity: A case study of aquatic vegetation. *Aquatic Sciences*, *81*(3), 41. https://doi.org/10.1007/s00027-019-0635-2

Lightbody, A. F., & Nepf, H. M. (2006). Prediction of velocity profiles and longitudinal dispersion in salt marsh vegetation. *Limnology and Oceanography*, *51*(1), 218–228. https://doi.org/10.4319/lo.2006.51.1.0218

Luhar, M., & Nepf, H. M. (2013). From the blade scale to the reach scale: A characterization of aquatic vegetative drag. *Advances in Water Resources*, *51*, 305–316. https://doi.org/10.1016/j.advwatres.2012.02.002

Marion, A., Nikora, V., Puijalon, S., Bouma, T., Koll, K., Ballio, F., Tait, S., Zaramella, M., Sukhodolov, A., O'Hare, M., Wharton, G., Aberle, J., Tregnaghi, M., Davies, P., Nepf, H., Parker, G., & Statzner, B. (2014). Aquatic interfaces: A hydrodynamic and ecological perspective. *Journal of Hydraulic Research*, *52*(6), 744–758. https://doi.org/10.1080/00221686.2014.968887

Marjoribanks, T. I., Lague, D., Hardy, R. J., Boothroyd, R. J., Leroux, J., Mony, C., & Puijalon, S. (2019). Flexural rigidity and shoot reconfiguration determine wake length behind saltmarsh vegetation patches. *Journal of Geophysical Research - Earth Surface*, *124*(8), 2176–2196. https://doi.org/10.1029/2019JF005012

Moore, R. D. (2005). Slug injection using salt in solution. *Streamline Watershed Management Bulletin*, *8*(2), 1–6.

Mrokowska, M., & Rowiński, P. M. (2017). Bed shear stresses and bed shear velocities—Ubiquitous variables in river hydraulics. In A. Radecki-Pawlik, S. Pagliara, & J. Hradecky (Eds.), *Open Channel hydraulics, river hydraulic structures and fluvial geomorphology: For engineers, geomorphologists and physical geographers* (pp. 180–195). CRC Press.

Mueller, D. S., Wagner, C. R., Rehmel, M. S., Oberg, K. A., & Rainville, F. (2013). Measuring discharge with acoustic Doppler current profilers from a moving boat. In *Measuring discharge with acoustic Doppler current profilers from a moving boat* (USGS Numbered Series No. 3-A22; Techniques and Methods) (Vol. 3-A22, p. 116). U.S. Geological Survey. https://doi.org/10.3133/tm3A22

Murphy, E., Ghisalberti, M., & Nepf, H. (2007). Model and laboratory study of dispersion in flows with submerged vegetation. *Water Resources Research*, *43*(5), 1–12. https://doi.org/10.1029/2006WR005229

O'Hare, M. T., Mountford, J. O., Maroto, J., & Gunn, I. D. M. (2016). Plant traits relevant to fluvial geomorphology and hydrological interactions. *River Research and Applications*, *32*(2), 179–189. https://doi.org/10.1002/rra.2940

Park, H., & Hwang, J. H. (2019). Quantification of vegetation arrangement and its effects on longitudinal dispersion in a channel. *Water Resources Research*, *55*(5), 4488–4498. https://doi.org/10.1029/2019WR024807

Parsons, D. R., Jackson, P. R., Czuba, J. A., Engel, F. L., Rhoads, B. L., Oberg, K. A., Best, J. L., Mueller, D. S., Johnson, K. K., & Riley, J. D. (2013). Velocity mapping toolbox (VMT): A processing and visualization suite for moving-vessel ADCP measurements. *Earth Surface Processes and Landforms*, *38*(11), 1244–1260. https://doi.org/10.1002/esp.3367

Perucca, E., Camporeale, C., & Ridolfi, L. (2009). Estimation of the dispersion coefficient in rivers with riparian vegetation. *Advances in Water Resources*, *32*(1), 78–87. https://doi.org/10.1016/j.advwatres.2008.10.007

Przyborowski, Ł., Łoboda, A. M., Bialik, R. J., & Västilä, K. (2019). Flow field downstream of individual aquatic plants—Experiments in a natural river with Potamogeton crispus L. and Myriophyllum spicatum L. *Hydrological Processes*, *33*(9), 1324–1337. https://doi.org/10.1002/hyp.13403

Rasmussen, J. J., Kallestrup, H., Thiemer, K., Alnøe, A. B., Henriksen, L. D., Larsen, S. E., & Baattrup-Pedersen, A. (2021). Effects of different weed cutting methods on physical and hydromorphological conditions in lowland streams. *Knowledge and Management of Aquatic Ecosystems*, *422*, 10. https://doi.org/10.1051/kmae/2021009

Rowiński, P. M., Okruszko, T., & Radecki-Pawlik, A. (2021). Environmental hydraulics research for river health: Recent advances and challenges. *Ecohydrology and Hydrobiology*, *22*, 213–225. https://doi.org/10.1016/j.ecohyd.2021.12.003

Rowiński, P. M., Västilä, K., Aberle, J., Järvelä, J., & Kalinowska, M. B. (2018). How vegetation can aid in coping with river management challenges: A brief review. *Ecohydrology & Hydrobiology*, *18*(4), 345–354. https://doi.org/10.1016/j.ecohyd.2018.07.003

Rutherford, J. C. (1994). *River mixing*. Wiley.

Schoelynck, J., Creëlle, S., Buis, K., De Mulder, T., Emsens, W.-J., Hein, T., Meire, D., Meire, P., Okruszko, T., Preiner, S., Roldan Gonzalez, R., Silinski, A., Temmerman, S., Troch, P., Van Oyen, T., Verschoren, V., Visser, F., Wang, C., Wolters, J.-W., & Folkard, A. (2018). What is a macrophyte patch? Patch identification in aquatic ecosystems and guidelines for consistent delineation. *Ecohydrology & Hydrobiology*, *18*(1), 1–9. https://doi.org/10.1016/j.ecohyd.2017.10.005

Shin, J., Seo, I. W., & Baek, D. (2020). Longitudinal and transverse dispersion coefficients of 2D contaminant transport model for mixing analysis in open channels. *Journal of Hydrology*, *583*, 124302. https://doi.org/10.1016/j.jhydrol.2019.124302

Shucksmith, J., Boxall, J., & Guymer, I. (2007). Importance of advective zone in longitudinal mixing experiments. *Acta Geophysica*, *55*(1), 95–103. https://doi.org/10.2478/s11600-006-0042-7

Shucksmith, J. D., Boxall, J. B., & Guymer, I. (2011). Determining longitudinal dispersion coefficients for submerged vegetated flow. *Water Resources Research*, *47*(10), 1–13. https://doi.org/10.1029/2011WR010547

Smith-Gill, S. J. (1975). Cytophysiological basis of disruptive pigmentary patterns in the leopard frog Rana pipiens. II. Wild type and mutant cell-specific patterns. *Journal of Morphology*, *146*(1), 35–54. https://doi.org/10.1002/jmor.1051460103

Sonnenwald, F., Hart, J. R., West, P., Stovin, V. R., & Guymer, I. (2017). Transverse and longitudinal mixing in real emergent vegetation at low velocities. *Water Resources Research*, *53*(1), 961–978. https://doi.org/10.1002/2016WR019937

Sonnenwald, F., Stovin, V., & Guymer, I. (2018). Use of drag coefficient to predict dispersion coefficients in emergent vegetation at low velocities. Proceedings of ISE, 2018. https://www.semanticscholar.org/paper/Use-of-drag-coefficient-to-predict-dispersion-in-at-Sonnenwald-Stovin/5b36691382e602af584b5624044989e92308a281

Sonnenwald, F., Stovin, V., & Guymer, I. (2019a). A stem spacing-based non-dimensional model for predicting longitudinal dispersion in low-density emergent vegetation. *Acta Geophysica*, *67*(3), 943–949. https://doi.org/10.1007/s11600-018-0217-z

Sonnenwald, F., Stovin, V., & Guymer, I. (2019b). Estimating drag coefficient for arrays of rigid cylinders representing emergent vegetation. *Journal of Hydraulic Research*, *57*(4), 591–597. https://doi.org/10.1080/00221686.2018.1494050

Tagwireyi, P., & Sullivan, S. M. P. (2015). Riverine landscape patch heterogeneity drives riparian ant assemblages in the Scioto River basin, USA. *PLoS One*, *10*(4), e0124807. https://doi.org/10.1371/journal.pone.0124807

Tang, X., & Knight, D. W. (2009). Analytical models for velocity distributions in open channel flows. *Journal of Hydraulic Research*, *47*(4), 418–428. https://doi.org/10.1080/00221686.2009.9522017

Thiemer, K., Schneider, S. C., & Demars, B. O. L. (2021). Mechanical removal of macrophytes in freshwater ecosystems: Implications for ecosystem structure and function. *Science of the Total Environment*, *782*, 146671. https://doi.org/10.1016/j.scitotenv.2021.146671

Västilä, K., & Järvelä, J. (2018). Characterizing natural riparian vegetation for modeling of flow and suspended sediment transport. *Journal of Soils and Sediments*, *18*(10), 3114–3130. https://doi.org/10.1007/s11368-017-1776-3

Västilä, K., Lee, C., Kim, D., Kim, S., Kim, J., & Järvelä, J. (2019). Measurement of lateral and wake flows associated with stream-scale willow patches. In L. Calvo (Ed.), *Proceedings, 38th IAHR world congress* (pp. 1–6). Panama City, Panama. https://doi.org/10.3850/38WC092019-1109

Västilä, K., Väisänen, S., Koskiaho, J., Lehtoranta, V., Karttunen, K., Kuussaari, M., Järvelä, J., & Koikkalainen, K. (2021). Agricultural water management using two-stage channels: Performance and policy recommendations based on northern European experiences. *Sustainability*, *13*(16), 9349. https://doi.org/10.3390/su13169349

Verschoren, V., Schoelynck, J., Cox, T., Schoutens, K., Temmerman, S., & Meire, P. (2017). Opposing effects of aquatic vegetation on hydraulic functioning and transport of dissolved and organic particulate matter in a lowland river: A field experiment. *Ecological Engineering*, *105*, 221–230. https://doi.org/10.1016/j.ecoleng.2017.04.064

Wang, Y., & Huai, W. (2016). Estimating the longitudinal dispersion coefficient in straight natural Rivers. *Journal of Hydraulic Engineering*, *142*(11), 04016048. https://doi.org/10.1061/(ASCE)HY.1943-7900.0001196

Wilcox, A. C., & Shafroth, P. B. (2013). Coupled hydrogeomorphic and woody-seedling responses to controlled flood releases in a dryland river. *Water Resources Research*, *49*(5), 2843–2860. https://doi.org/10.1002/wrcr.20256

Xu, Y., & Nepf, H. (2020). Measured and predicted turbulent kinetic energy in flow through emergent vegetation with real plant morphology. *Water Resources Research*, *56*(12), e2020WR027892. https://doi.org/10.1029/2020WR027892

Yamasaki, T. N., de Lima, P. H. S., Silva, D. F., Preza, C. G. d. A., Janzen, J. G., & Nepf, H. M. (2019). From patch to channel scale: The evolution of emergent vegetation in a channel. *Advances in Water Resources*, *129*, 131–145. https://doi.org/10.1016/j.advwatres.2019.05.009

Young, P., Jakeman, A., & McMurtrie, R. (1980). An instrumental variable method for model order identification. *Automatica*, *16*(3), 281–294. https://doi.org/10.1016/0005-1098(80)90037-0

Zeng, Y., & Huai, W. (2014). Estimation of longitudinal dispersion coefficient in rivers. *Journal of Hydro-Environment Research*, *8*(1), 2–8. https://doi.org/10.1016/j.jher.2013.02.005

SUPPORTING INFORMATION

Additional supporting information may be found in the online version of the article at the publisher's website.